Title
ANALYZING POWERS FOR TWO-NUCLEON TRANSFER REACTIONS IN THE lp-SHELL

Authors
Macdonald, J.A.
Cerny, Joseph
Hardy, J.C.
et al.

Publication Date
1973-10-01

Submitted to Physical Review C

LBL-2317
Preprint

ANALYZING POWERS FOR TWO-NUCLEON TRANSFER REACTIONS IN THE 1p-SHELL

J. A. Macdonald, Joseph Cerny, J. C. Hardy, H. L. Harney,
A. D. Bacher and G. R. Plattner

October 1973

Prepared for the U. S. Atomic Energy Commission
under Contract W-7405-ENG-48

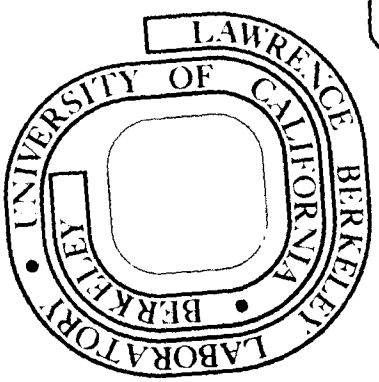

DISCLAIMER

ANALYZING POWERS FOR TWO-NUCLEON TRANSFER REACTIONS IN THE 1p-SHELL*

J. A. Macdonald†, Joseph Cerny, J. C. Hardy†, H. L. Harney‡, A. D. Bacher‡‡, and G. R. Plattner‡

Department of Chemistry and
Lawrence Berkeley Laboratory
University of California
Berkeley, California 94720

October 1973

ABSTRACT

The $(\vec{p},t)$ and $(\vec{p},{}^3He)$ reactions have been induced on ^{16}O, ^{15}N, and ^{13}C targets by polarized protons of 43.8 or 49.6 MeV. Relative differential cross sections and analyzing powers were measured for thirty-two transitions and compared with zero-range DWBA calculations employing Cohen and Kurath wave functions. Although good results for differential cross sections were obtained, attempts to fit analyzing powers were less successful. In general $(\vec{p},t)$ results gave better agreement than $(\vec{p},{}^3He)$, ground state transitions better than those to excited states, and transitions to analog states better than more complex transitions.

I. INTRODUCTION

The two-nucleon transfer reactions (p,t) and (p,^{3}He) have become well established as valuable spectroscopic tools in characterizing nuclear energy levels, e.g., Ref. 1,2. Many of these results have been the consequence of theoretical interpretation of differential cross sections in terms of the distorted wave Born approximation (DWBA) incorporating shell model nuclear wave functions.[3] With the advent of polarized ion sources capable of high quality polarized proton beams, it has also become possible to measure the analyzing powers for these reactions with little added experimental difficulty. The data obtained in such experiments constitute an important further test for the reaction theory as well as for the nuclear structure of the states involved. Some limited previous results on ^{16}O, ^{12}C, and ^{28}Si targets have already been reported by Nelson et al.[4,5]

The relatively simple zero-range DWBA has enjoyed considerable success in describing the angular distributions of (p,t) and (p,^{3}He) reactions at forward angles ($\theta_{lab} \leqslant 60°$), see e.g., Ref. 6. For this reason one might expect this model to adequately describe the experimental analyzing powers as well, since both quantities are simply related to the transition amplitude. However, previous reports[7] of major inconsistencies between experiment and theory in the ratios of cross sections to certain mirror pairs is already evidence of some inadequacy in describing these two-nucleon transfer reactions with the simple DWBA, so that general comparisons of theoretical with experimental analyzing powers are of interest.

At the outset of this present work the hope was that the analyzing powers of simple ($\vec{p}$,t) transitions would be well described by the DWBA, so that

one might obtain further insight into the more complex transitions, and as a result shed some light on such problems as the inconsistent cross section ratios. Early analysis[8] of part of these data, however, produced the result that in a number of unique L = 2 transitions, all characterized by similar differential cross section angular distributions, the analyzing powers were not all similar, nor were they all reproduced by the DWBA. In this paper, we present a more complete report, giving our results for the analyzing powers of $(\vec{p},t)$ and $(\vec{p},{}^3He)$ reactions on targets of ^{16}O, ^{15}N, and ^{13}C.

II. EXPERIMENT

The experiments were performed at the Lawrence Berkeley Laboratory 88-inch cyclotron, using the axial injection polarized ion source.[9] The source is of the atomic-beam type and the polarization vector of the protons along the y-axis, which is defined as being perpendicular to the beam (z) direction[10] and the reaction plane, could be reversed by reversing the current in the strong-field ionizer solenoid. Beam polarizations of $|p_y| \simeq 75$-80% can be routinely achieved for protons with a beam current between 10 and 50 nA. For ^{16}O and ^{15}N targets, a beam energy of 43.8 MeV was used; for ^{13}C the energy was 49.6 MeV.

After passing through the target, the beam was recollimated before entering a polarimeter located downstream from the main scattering chamber. For measurements at 49.6 MeV, the beam was degraded by an aluminum absorber to 40 MeV before entering the polarimeter since it was not calibrated at the higher energy. The polarimeter was a second, smaller scattering chamber with ^4He contained at $\sim$ 1 atm pressure in a gas cell with 5 μm Havar foil windows. Elastic scattering of the beam particles on ^4He was observed in two counter telescopes symmetrically oriented on opposite sides of the beam axis.

In this way, from the known analyzing power for p-α scattering,[11] the beam polarization could be continuously measured. The beam was then stopped in a split Faraday cup connected to two current meters feeding a single integrating electrometer. Centering of the beam, which was monitored in the split Faraday cup and by a pair of electrically isolated collimators in front of the target, could be controlled and maintained by a small steering magnet ~ 4 m upstream from the scattering chamber.

Each target gas - O_2, N_2, and CH_4 - was contained at typically 200 Torr in a cell with 5 μm Havar windows. The ^{15}N was isotopically enriched to 99% and the ^{13}C to 93%. Data, which will be reported later,[12] were also obtained on ^{7}Li and ^{9}Be self-supporting solid targets.

Outgoing light reaction products were detected in four nearly identical semiconductor counter telescopes arranged in two pairs located symmetrically about the beam axis. This allowed measurement of left and right spectra simultaneously at two angles separated by 10°. Each counter telescope consisted of a phosphorus-diffused ΔE- and a lithium-drifted E-detector. The ΔE detectors were 110-140 μm thick and the E detectors were 3-5 mm, depending on the kinematics of the particular experiment. The double collimators were such that the angular acceptance was about 1° and the solid angle about 1×10^{-4} sr. In addition, two single 5 mm monitor detectors were located in the scattering chamber 10° above the horizontal beam plane at $\theta_{lab} = \pm 8°$. These detectors were used to normalize relative differential cross-sections since the polarimeter prevented complete integration of the incident beam current.

For each of the six telescopes (two in the polarimeter, four in the scattering chamber) the ΔE and E signals were fed through charge sensitive

pre-amplifiers to remotely located linear amplifiers. After satisfying mutual coincidence requirements ($2\tau \sim 100$ nsec), these signals were fed to a Goulding-Landis particle identifier.[13] Total energy signals from identified tritons and ^{3}He's were then routed to a 4096 channel analyzer operated in 16×256 channel mode. Since reactions induced by protons of both spin orientations were taken at each angle, all the triton and ^{3}He spectra from all four systems for both spin orientations were thereby collected in the analyzer before being stored on magnetic tape for subsequent computer analysis.

In all the cases studied, spectra had previously been reported from unpolarized (p,t) and (p,^{3}He) experiments. Our data were first compared to the earlier work to confirm excitation energies and relative differential cross-sections. The latter were obtained for each transition by normalization of the sum of the appropriate peak from the left and right systems to the monitors mentioned above. Absolute magnitudes were then obtained by a suitable single normalization of the data from each target to the previous unpolarized work in the literature,[1,2,6,7] with which good agreement was observed.

The data were then analyzed to determine asymmetries and analyzing powers. The asymmetry is defined by $e_y = \frac{1 - r}{1 + r}$, where $r = [(\frac{N_R^{\uparrow}}{N_L^{\uparrow}}) \cdot (\frac{N_L^{\downarrow}}{N_R^{\downarrow}})]^{1/2}$ and N_i^j is the number of counts (less background) under the peak of interest on the i^{th} side (i.e., left or right) of the beam axis for an incident beam of spin orientation j (up or down). Such a geometrical mean removes, in first order, the effects of any systematic instrumental asymmetry.[14] The quantity e_y depends only on the analyzing power, A_y, of the transition and the beam polarization, p_y:

$$p_y \cdot A_y = e_y$$

Although the experimental apparatus was carefully aligned to minimize instrumental asymmetry, a further check on the data was performed; the quantity $\Omega = (\frac{N_R^{\uparrow}}{N_L^{\uparrow}} \cdot \frac{N_R^{\downarrow}}{N_L^{\downarrow}})^{1/2}$ was evaluated for each measurement and was determined to be statistically constant and approximately unity.

Our results for A_y include error bars which reflect the statistical uncertainties in the peak integrations and in the backgrounds, as well as the uncertainty in the determination of the beam polarization, which was, in general, small compared to either of the first two.

III. DWBA CALCULATIONS

Detailed discussions of two-nucleon DWBA theory exist elsewhere.[3,15] For the purposes of this paper, therefore, only a brief summary will be presented. A pick-up transition between a target A and a residual nucleus B can be characterized by a transition amplitude $T_{fi}(J_A M_A \mu_i \rightarrow J_B M_B \mu_f)$ where J, M, and μ are the total angular momentum, total angular momentum projection and light particle spin projection, respectively. The differential cross section is then

$$(\frac{d\sigma}{d\Omega}) \propto \sum_{M_A M_B \mu_i \mu_f} |T_{fi}|^2 \qquad (1)$$

For a transition involving a spin-dependent interaction potential, such as in the case for distorted waves generated by optical potentials including a spin-orbit term, the differential cross section can be written

$$(\frac{d\sigma}{d\Omega}) \propto \sum_{M\mu_i\mu_f}^{J} |\sum^{\gamma LST} G_{\gamma LSJT} B^{LSJT}_{M\mu_i\mu_f}|^2 \qquad (2)$$

where LSJT are the quantum numbers of the transferred pair, γ stands for the configurations of the transferred nucleons ($[n_1\ell_1 j_1]\ [n_2\ell_2 j_2]$; JT), G is a spectroscopic or structure amplitude, including a spectroscopic factor for the light particles, and B is a kinematic and angular momentum transfer amplitude. If the spatial part of the wave function of the two nucleons in state γ is transformed to relative and center-of-mass coordinates and the relative motion is assumed to be pure S-state, then the differential cross section takes the form

$$\left(\frac{d\sigma}{d\Omega}\right) \propto \sum_{M\mu_i\mu_f}^{J} \left| \sum^{LST} \sum^{N} G_{NLSJT}\, B^{LSJT}_{M\mu_i\mu_f} \right|^2 \qquad (3)$$

where N is the principal quantum number of the center-of-mass motion.

In order to evaluate the structure amplitude, it is necessary to obtain the wave function for the center-of-mass motion of the transferred nucleons as they appear in the target nucleus and project out that component for which their relative motion is the same as that found for the corresponding nucleons in the triton (for (p,t) reactions) or in the ^{3}He particle (for (p,^{3}He)). The structure amplitudes arise as coefficients in the expansion of the "projected" two-nucleon radial wave function, $\tilde{\psi}$, in terms of harmonic oscillator basis states, u:

$$\tilde{\psi}_{SJT}(R) = \sum^{LN} G_{NLSJT}\, u_{NL}(2\nu R^2) \qquad (4)$$

Amplitudes $G_{NLSJT}(jj')$ have been tabulated by Glendenning[15] for the transfer of nucleons from pure (jj') configurations.

Since Cohen and Kurath[16] have evaluated two particle fractional parentage factors $\beta_{jj'SJT}$ between various nuclear states in the 1p shell from their effective-interaction shell model calculations, our spectroscopic amplitudes have generally been evaluated as follows:

$$G_{NLSJT} = \sum_{jj'} \beta_{jj'SJT}\, G_{NLSJT}(jj') \qquad (5)$$

For negative parity states in mass-14, simple shell model configurations based on the calculations of True[17] were assumed. In all cases, the tabulated structure amplitudes[15] were corrected to an oscillator parameter $\nu = 0.32$. The harmonic oscillator form factor itself was modified by matching it at large radius to a Hankel function whose asymptotic behavior corresponded to the experimental two-nucleon binding energy.

The nature of the analyzing power can best be visualized for a $(\vec{p},t)$ transition, for example, by considering the reverse $(t,\vec{p})$ reaction. Time reversal invariance requires that the analyzing power in the former be equal to the polarization of the outgoing protons in the latter if the reaction is induced by an unpolarized triton beam. We denote the two projections of a spin 1/2 particle by + and -; then, in terms of the transition amplitude, the probability that the outcoming proton will have spin $\overset{+}{(-)}$ is

$$\sigma_{\overset{+}{(-)}} \propto \sum_{M_A M_B \mu_t} |T_{fi}(M_B \mu_t \rightarrow M_A \mu_p \overset{+}{(-)})|^2 \quad . \qquad (6)$$

The polarization p is defined as

$$p \equiv \frac{\sigma_+ - \sigma_-}{\sigma_+ + \sigma_-} \quad . \qquad (7)$$

Without reproducing the complete selection rules for these reactions we note that for spin 0 and 1/2 targets, a (p,t) transition is characterized by

a single value for the transferred orbital angular momentum L; a $(p,{}^3He)$ transition is characterized by one or more sets of transferred quantum numbers L, S, and J. In both cases the parity change is $\Delta\pi = (-1)^L$. As can be seen from Eq. (3), the differential cross-section involves a coherent sum over L and S and an incoherent sum over J. We adopt the following notation for characterizing a complex $(p,{}^3He)$ transition:

$$(J/L/S) = (J_1/L_{11}, L_{12}, \ldots/S_{11}, S_{12}, \ldots) \quad ,$$

$$(J_2/L_{21}, L_{22}, \ldots/S_{21}, S_{22}, \ldots) \quad , \ldots$$

where parentheses indicate a coherent sum over the indicated L_{ij} and S_{ik} to give the J_i, and that the cross-sections for the J_i are then added incoherently according to Eq. (3). Therefore, as an example:

$$(J/L/S) = (2/2/0,1),\ (3/2/1) \text{ implies } \frac{d\sigma}{d\Omega} \propto \sum_{J=2,3} \left| \sum_{\substack{L=2 \\ S=0,1}} \right|^2 \quad .$$

It has been shown[6,7] that the spin-dependence in the interaction potential in $(p,{}^3He)$ transitions results in a relative strength for S = 0 *vs.* S = 1 transfer amplitudes of about 1.7:1. In the calculations, we have included this effect which amounts to a reduction of S = 1 character in the differential cross section by a factor of three relative to S = 0.

Zero-range DWBA calculations predicting differential cross-sections and analyzing powers for the reactions on ^{16}O, ^{15}N, and ^{13}C targets were performed using the program DWUCK.[18] This code included a spin-orbit distortion in the optical potentials. The optical model parameters for the protons and mass-3

particles are summarized in Table I. The potentials shown do not include a spin-orbit strength in the exit (mass-3) channel. A survey of the effects of including such a potential indicated that only minor changes in the analyzing power calculations resulted.[8,12] As a consequence, the mass-3 spin-orbit potential was omitted for simplicity in the calculations presented here.

IV. RESULTS AND DISCUSSION

A. Comparison of Analog Transitions

In this work angular distributions have been measured for four pairs of T = 1 analog (p,t) and (p,^{3}He) transitions. The data for their analyzing powers, which are shown in Fig. 1, illustrate clearly the well known similarity between the two members of each pair. Each of these transitions will be further discussed later.

B. ^{16}O($\vec{p}$,t) and ($\vec{p}$,^{3}He)

Typical spectra of identified tritons and ^{3}He's showing states in ^{14}O and ^{14}N, respectively, are shown in Fig. 2. Because the target spin is 0^+, all reactions on this nucleus transfer unique J, and in the case of ($\vec{p}$,t) this also implies unique L = J. For ($\vec{p}$,^{3}He) at most two L values can contribute to each transition.

Angular distribution data for the ^{16}O($\vec{p}$,t)^{14}O reaction are summarized in Fig. 3. Good agreement between experimental and theoretical differential cross sections is evident for the L = 0 ground state transition and for the L = 2 transitions to states in ^{14}O at 6.59, 7.78, and 9.72 MeV. However, for the analyzing power angular distributions the theory predicts similar shapes for all three L = 2 transitions while the data indicate that the transition to the

6.59 MeV state differs significantly both from the prediction and from the other two transitions which agree rather well with the theory.

The weak transitions to the negative parity states at 5.17 MeV (1^-) and 6.29 MeV (3^-) show little similarity to the calculated angular distributions. From equivalent results for cross section data alone, Fleming et al.[6] concluded that an unambiguous L transfer assignment could not be made to the transition to the 6.29 MeV state. Evidently the analyzing power data do nothing to alter that conclusion.

The $^{16}O(\vec{p},^3He)^{14}N$ results are shown in Fig. 4. Of particular interest are the 1^+ states in ^{14}N at 0 and 3.95 MeV. Both transitions can go by L = 0 or 2 but the cfp's of Cohen and Kurath[16] indicate predominant L = 2 to the ground state and L = 0 to the 3.95 MeV state; the data for $\frac{d\sigma}{d\Omega}$ clearly support this prediction, although the agreement is only qualitative for the 3.95 MeV transition. However, there is no agreement whatsoever for the A_y in either case, which is particularly surprising for the ground state whose $\frac{d\sigma}{d\Omega}$ is well fit. It is worth noting that the predominantly L = 0 theoretical fit to the 3.95 MeV 1^+ state would approximate a reasonable qualitative fit to the ground state transition A_y. In an effort to vary the details of the wave functions to determine the magnitude of the effect on A_y, calculations were carried out using structure factors corresponding to a pure jj configuration;[21] no major changes resulted and it seems unlikely that the simple DWBA is capable of resolving this discrepancy.

The 5.11 MeV (2^-) state should presumably be populated by L = 1 or L = 3 transfer. Since detailed cfp's were not available for this transition, separate computations for each allowed L-value are shown in Fig. 4. The $\frac{d\sigma}{d\Omega}$ data clearly indicate dominant L = 3 but this is not confirmed by the measurements for A_y, which agree with neither L = 1 nor L = 3.

The 2^+ states at 7.03 and 9.17 MeV are T = 0 and T = 1, respectively, the latter being the analog of the 6.59 MeV 2^+ state in ^{14}O. Figure 4 shows rather good DWBA agreement with the experimental $\frac{d\sigma}{d\Omega}$ for both of these, primarily at forward angles for the T = 0 state. The calculated A_y for the T = 0 state is also in reasonable qualitative agreement with the data. However, the A_y measurements for the T = 1 state, as for its analog in ^{14}O, disagree with the calculations and are out of phase with the other observed L = 2 transitions.

C. $^{15}N(\vec{p},t)$ and $(\vec{p},^3He)$

Figure 5 shows examples of ^{13}N and ^{13}C spectra obtained from the ^{15}N target. In this case, the corresponding $(\vec{p},t)$ and $(\vec{p},^3He)$ reactions yield pairs of mirror states in the final nuclei, as well as T = 3/2 analogs at ~ 15 MeV. Since the spin of the target is 1/2-, the selection rules permit up to four combinations of transferred (J/L/S) for the $(\vec{p},^3He)$ case as shown in Table II, although the $(\vec{p},t)$ transitions remain unique.

The $(\vec{p},t)$ angular distributions appear in Fig. 6. The L = 0 ground state transition bears a strong resemblance to the L = 0 analog transitions induced on ^{16}O (Figs. 3 and 4), and agrees equally well with the DWBA calculations. The three L = 2 transitions have similar $\frac{d\sigma}{d\Omega}$ shapes and also agree with the DWBA, particularly at forward angles. However, here the theory also predicts similar A_y angular distributions, but the data indicate no such uniformity. The transition to the 3.51 MeV state agrees very poorly, while that to the 7.38 MeV state is reproduced rather well. The large error bars for the transition to the 15.07 MeV T = 3/2 state make the comparison of theoretical and experimental A_y inconclusive, although it appears that the agreement is not good.

The $^{15}N(\vec{p},^3He)^{13}C$ results are shown in Fig. 7. Although these transitions lead to states in ^{13}C which are mirrors of the ^{13}N states, the increased

complexity permitted in the $(\vec{p},{}^3He)$ reaction makes it unlikely that either the $\frac{d\sigma}{d\Omega}$ or the A_y to such mirror states would be identical with the $(\vec{p},t)$ data. The transitions to the ground and first excited states both go by mixed L = 0,2 and the wave functions indicate similar mixtures of L in both. The $\frac{d\sigma}{d\Omega}$ data indeed are in reasonable agreement with the theory. For the A_y data, the theory again suggests that these two transitions should be comparable, and the data show some similarity, particularly at forward angles, but only fair agreement with the calculation in the same region. At angles beyond 30° c.m. neither transition agrees with the theory although they do maintain similar shapes out to nearly 50° c.m.

For the 7.55 MeV (5/2-) state the selection rules allow L = 2 and 4 but L = 4 is excluded in p-shell pick-up. In spite of the multiple J-transfer still allowed (see Table II), the transition is expected to exhibit a pure L = 2 shape, which is confirmed by the $\frac{d\sigma}{d\Omega}$ results. However, for the analyzing power, both the calculations and the experimental results exhibit an angular distribution shape quite different from that for any of the pure L = 2 transitions arising in $(\vec{p},t)$, yet at the same time experiment and theory do not agree quantitatively with one another.

The $(\vec{p},{}^3He)$ transition to the ^{13}C state at 15.11 MeV (3/2-, T = 3/2) is also shown in Fig. 7. Good DWBA agreement for $\frac{d\sigma}{d\Omega}$ was obtained, although the angular range for detecting ^3He's from transitions to states at this high excitation was restricted by the thickness of the ΔE detectors. Again, as with the $(\vec{p},t)$ analog, the A_y comparison with theory is not definitive because of the large experimental error-bars.

D. $^{13}C(\vec{p},t)$ and $(\vec{p},^3He)$

Representative $(\vec{p},t)$ and $(\vec{p},^3He)$ spectra showing final states in ^{11}C and ^{11}B are shown in Fig. 8. The $\frac{d\sigma}{d\Omega}$ and A_y data and calculations for the mirror transitions and the T = 3/2 analogs are shown in Figs. 9 and 10.

Three L = 2 $(\vec{p},t)$ transitions to the ground (3/2-), 4.31 MeV (5/2-) and 4.79 MeV (3/2-) states are shown in Fig. 9. While detailed agreement for $\frac{d\sigma}{d\Omega}$ with the DWBA is not achieved, there is reasonable overall agreement. For the analyzing powers, the agreement with the ground state transition is excellent, and with the two other states it is at least qualitatively satisfactory. Certainly, compared with the L = 2 disagreements for the ^{16}O and ^{15}N data, there are no dramatic discrepancies here.

A striking comparison with the results on the ^{15}N and ^{16}O targets occurs for the pure L = 0 transition to the 2.00 MeV (1/2-) state in ^{11}C. Again the $\frac{d\sigma}{d\Omega}$ is in qualitative agreement, but the A_y shows no similarity whatsoever, whereas rather good L = 0 agreement was obtained for both the other targets. Here, the choice of optical potentials was found to have an important influence on the shape of the calculated angular distribution, but improvement in the A_y calculation was always at the expense of the $\frac{d\sigma}{d\Omega}$ agreement for the same state as well as the overall agreement for the ground state transition. In contrast, for the other L = 0 transition (to the 12.47 MeV state), although detailed fits to both $\frac{d\sigma}{d\Omega}$ and A_y are not obtained, the qualitative features of both are reasonably well reproduced.

The $(\vec{p},t)$ transition to the 6.48 MeV (7/2-) state in ^{11}C is L-forbidden, if simple p-shell pick-up of the two neutrons is assumed. Two explanations for the surprisingly large strength of the transition have been proposed.[7] The first

assumes that a two-step mechanism plays a major role in the pick-up, involving an allowed L = 2 process, and the second hypothesizes that a small admixture of (1p 1f) structure in the ^{13}C ground state would account for the observed strength and permit the necessary L = 4 transfer. Calculations showing pure L = 2 and L = 4 transfer are shown with the data for $\frac{d\sigma}{d\Omega}$ and A_y in Fig. 9. It is apparent that some suitable admixture of L = 2 and 4 might account for the nearly isotropic $\frac{d\sigma}{d\Omega}$, but the results for A_y, if believable here, prefer L = 2. These results do not resolve the questions about this unusual transition but may indicate the presence of an allowed L = 2 process.

The $^{13}C(\vec{p},^3He)$ transfers leading to states in ^{11}B which are mirrors of the ^{11}C states already discussed are shown in Fig. 10. As for the ^{15}N target, $(\vec{p},^3He)$ on ^{13}C is allowed to proceed in general through a complex admixture of transferred (J/L/S). Though the theory reproduces $\frac{d\sigma}{d\Omega}$ rather well for all these transitions, no agreement is obtained for A_y with the exception of the 12.94 MeV (1/2-, T = 3/2) transition where fair qualitative agreement is obtained. The calculation for the 6.74 MeV (7/2-) transition (allowed in $(\vec{p},^3He)$) too is qualitatively correct, but the magnitude is wrong by nearly a factor of two.

V. SUMMARY

In this work we have measured angular distributions and analyzing powers for a large number of $(\vec{p},t)$ and $(\vec{p},^3He)$ transitions in 1p-shell nuclei. In agreement with previous work, we have seen that cross section angular distributions for transitions that involve a unique transferred L-value (i.e., the $(\vec{p},t)$ transitions and some of the $(\vec{p},^3He)$ transitions) exhibit characteristic shapes. Unfortunately, the analyzing powers do not. The situation is even more complex in the remaining $(\vec{p},^3He)$ transitions since they possess greater flexibility in the transferred spin and isospin.

In order to provide some initial theoretical perspective on these results, the data have been compared with DWBA calculations incorporating spin-orbit terms in the optical potentials and the zero-range approximation. For these lp-shell transitions involving a single L-transfer, the DWBA calculations suggest that the analyzing power is often, but not always, characteristic of this L-value. Unfortunately, comparison with experiment indicates that only in some of the particularly simple transitions, such as $(\vec{p},t)$ reactions to ground and analog final states, does this simple DWBA approach give an acceptable account of the data. In a large number of other apparently uncomplicated transitions the DWBA completely fails to predict the analyzing powers. It is apparent that the analyzing powers are sensitive to details which have only a minimal effect on the shape of the differential cross sections.

There is no doubt that a major factor contributing to this difficulty is the choice of suitable optical potentials. For these targets and energies, the choice is not always obvious, especially for the mass-3 channel. Given the lack of complete optical model information for the applicable elastic scattering processes, this source of uncertainty cannot be overcome.

A substantial effort has been made by a number of workers (e.g., Ref. 22) to modify the DWBA formalism to eliminate the need for the zero-range approximation. With respect to analyzing powers, Nelson et al.[5] have had some success in improving fits to the few cases they considered by including a finite range routine, but it is not at all obvious that the large changes needed to achieve good agreement with some of the data presented here could be obtained in this way. Certainly, it would be very interesting to examine this approach with the more extensive experimental data now available.

By assuming a simple direct process in these calculations, the effects of multiple-step processes have been neglected. The extent to which such factors affect the analyzing power in these cases is not known and should also be examined. The strength of the L-forbidden $(\vec{p},t)$ transition on the ^{13}C target is a good indication that the assumption of a one-step direct mechanism may be too simplistic in some circumstances.

The lack of success in fitting the analyzing power for so many of these 1p-shell transitions using this DWBA approach differs from the recent results[23] of an investigation of the $^{208}Pb(\vec{p},t)^{206}Pb$ reaction at 40 MeV, which observed the ground (0^+), 0.80 MeV (2^+), 1.68 MeV (4^+) and 3.25 MeV (6^+) states. For this heavy target, excellent agreement for the differential cross sections and rather good overall agreement for the analyzing powers was achieved. Obviously, our results on 1p-shell targets indicate a clear need for further theoretical effort, and these data should provide a sensitive test of new theoretical developments in the study of two-nucleon transfer reactions in light nuclei.

One of us (J.A.M.) wishes to gratefully acknowledge a Postgraduate Scholarship granted by the National Research Council of Canada.

FOOTNOTES AND REFERENCES

*Work performed under the auspices of the U. S. Atomic Energy Commission.

†Present address: Chalk River Nuclear Laboratories, AECL, Chalk River, Ontario KOJ 1JO, Canada.

‡Present address: Max-Planck-Institut für Kernphysik, Heidelberg, West Germany.

‡‡Present address: Physics Department, Indiana University, Bloomington, Indiana 47401.

‡Present address: University of Basel, Basel, Switzerland.

1. J. Cerny and R. H. Pehl, Phys. Rev. Letters 12, 619 (1964).
2. D. G. Fleming, J. Cerny, C. C. Maples, and N. K. Glendenning, Phys. Rev. 166, 1012 (1968).
3. I. S. Towner and J. C. Hardy, Advan. Phys. 18, 401 (1969).
4. J. M. Nelson, N. S. Chant, and P. S. Fisher, Phys. Letters 31B, 445 (1970).
5. J. M. Nelson, N. S. Chant, and P. S. Fisher, Nucl. Phys. A156, 406 (1970).
6. D. G. Fleming, J. C. Hardy, and J. Cerny, Nucl. Phys. A162, 225 (1971).
7. D. G. Fleming, J. Cerny, and N. K. Glendenning, Phys. Rev. 165, 1153 (1968).
8. J. C. Hardy, A. D. Bacher, G. R. Plattner, J. A. Macdonald, and R. G. Sextro, Phys. Rev. Letters 25, 298 (1970).
9. D. J. Clark, A. U. Luccio, F. Resmini, and H. Meiner, Fifth International Cyclotron Conference, Oxford, England, 1969, ed. R. W. McIlroy, (Butterworth & Co., Ltd., London, 1971), p. 610.
10. Our nomenclature and definitions follow the Madison Convention, Polarization Phenomena in Nuclear Reactions, Proc. Third International Symposium, Madison, 1970, ed. H. H. Barschall and W. Haeberli, (University of Wisconsin, Madison, 1971), p. xxv.

11. A. D. Bacher, G. R. Plattner, H. E. Conzett, D. J. Clark, H. Grunder, and W. F. Tivol, Phys. Rev. C5, 1147 (1972).

12. J. A. Macdonald, Ph.D. Thesis, University of California, Berkeley, Lawrence Berkeley Laboratory Report LBL-2320, 1973 (unpublished).

13. F. S. Goulding, D. A. Landis, J. Cerny, and R. H. Pehl, Nucl. Instr. Methods 31, 1 (1964).

14. G. R. Plattner, T. B. Clegg, and L. G. Keller, Nucl. Phys. A111, 481 (1968).

15. N. K. Glendenning, Ann. Rev. Nucl. Sci. 13, 191 (1963); Phys. Rev. 137, B102 (1965); University of California, Lawrence Berkeley Laboratory Reports UCRL-18268 and UCRL-18269 (unpublished).

16. S. Cohen and D. Kurath, Nucl. Phys. A141, 145 (1970).

17. W. W. True, Phys. Rev. 130, 1530 (1963).

18. Written by P. D. Kunz, Oct. 1967 version. The modifications to include the harmonic oscillator form factor and coherent and incoherent summation were made by us.

19. F. Ajzenberg-Selove and T. Lauritsen, Nucl. Phys. A114, 1 (1968); F. Ajzenberg-Selove, Nucl. Phys. A152, 1 (1970).

20. S. W. Cosper, R. L. McGrath, J. Cerny, C. C. Maples, G. W. Goth, and D. G. Fleming, Phys. Rev. 176, 1113 (1968).

21. Structure amplitudes corresponding to a pure jj-configuration were taken from Ref. 6.

22. N. Austern, R. M. Drisko, E. C. Halbert, and G. R. Satchler, Phys. Rev. 133, B3 (1964); E. Rost and P. D. Kunz, Nucl. Phys. A162, 376 (1971); L. A. Charlton, Phys. Rev. C8, 146 (1973).

23. J. A. Macdonald, N. A. Jelley, and J. Cerny, Phys. Letters (in press).

Table I. Optical Model Parameters[a] Used in DWBA

Target	Particle	V_0 (MeV)	W_0 (MeV)	W_1 (MeV)	V_S (MeV)	r_0 (fm)	r_0' (fm)	r_s (fm)	r_c (fm)	a (fm)	a' (fm)	a_s (fm)	Ref.
$^{15}N, ^{16}O$	proton (43.8 MeV)	44.53	17.51	6.51	6.20	1.141	1.26	1.066	1.3	0.715	0.64	0.674	b
	mass-3	220.0	23.8	--	--	1.22	1.80	--	1.3	0.530	0.990	--	c
^{13}C	proton (49.6 MeV)	38.38	21.49	3.81	5.75	1.141	1.26	1.066	1.3	0.715	0.64	0.674	b
	mass-3	160.0	14.86	--	--	1.31	1.73	--	1.3	0.565	0.826	--	d

[a]The optical potential was defined as:

$$V(r) = V_c(r) - V_0\left(\frac{1}{e^x + 1}\right) - iW_0\left(\frac{1}{e^{x'} + 1}\right) - iW_1 e^{-x'^2} - \left(\frac{\hbar}{M_\pi c}\right)^2 V_S \frac{1}{r}\frac{d}{dr}\left(\frac{1}{e^{x_s} + 1}\right) \vec{\sigma} \cdot \vec{\ell}$$

where $V_c(r)$ is the Coulomb potential for a uniformly charged sphere of radius $r_c A^{1/3}$ fm;

$x = (r - r_0 A^{1/3})/a$, $x' = (r - r_0' A^{1/3})/a'$ and $x_s = (r - r_s A^{1/3})/a_s$.

[b]Quoted in Ref. 6 for proton elastic scattering on ^{16}O at 43.1 MeV.

[c]Quoted in Ref. 6 for ^3He elastic scattering on ^{12}C at 30.0 MeV.

[d]From a compilation by C. M. Perey and F. G. Perey, Nucl. Data Tables 10, 539 (1972).

Table II. Summary of Two-Nucleon Pick-up Transitions

Target J^π,T	$E_p^{\rightarrow}$ [a]	$(\vec{p},t)$			$(\vec{p},{}^3He)$		
		Final State (MeV)	J^π,T [b]	L	Final State (MeV)	J^π,T [b]	(J/L/S)
^{16}O $0^+,0$	43.8	^{14}O			^{14}N		
		g.s.	$0^+,1$	0	g.s.	$1^+,0$	(1/0,2/1)
		5.17[c]	$(1^-),1$	1	2.31	$0^+,1$	(0/0/0)
		6.29[c]	$(3^-),1$	3	3.95	$1^+,0$	(1/0,2/1)
		6.59	$2^+,1$	2	5.11[c]	$2^-,0$	(2/1,3/1)
		7.78	$2^+,1$	2	7.03	$2^+,0$	(2/2/1)
		9.72	$(2^+),1$	2	9.17	$2^+,1$	(2/2/0)
^{15}N $1/2^-,1/2$	43.8	^{13}N			^{13}C		
		g.s.	$1/2^-,1/2$	0	g.s.	$1/2^-,1/2$	(0/0/0), (1/0,2/1)
		3.51	$3/2^-,1/2$	2	3.68	$3/2^-,1/2$	(1/0,2/1), (2/2/0,1)
		7.39	$5/2^-,1/2$	2	7.55	$5/2^-,1/2$	(2/2/0,1), (3/2/1)
		15.07	$3/2^-,3/2$	2	15.11	$3/2^-,3/2$	(2/2/0)
^{13}C $1/2^-,1/2$	49.6	^{11}C			^{11}B		
		g.s.	$3/2^-,1/2$	2	g.s.	$3/2^-,1/2$	(1/0,2/1), (2/2/0,1)
		2.00	$1/2^-,1/2$	0	2.12	$1/2^-,1/2$	(0/0/0), (1/0,2/0)
		4.31	$5/2^-,1/2$	2	4.44	$5/2^-,1/2$	(2/2/0,1), (3/2/1)
		4.79	$3/2^-,1/2$	2	5.02	$3/2^-,1/2$	(1/0,2/1), (2/2/0,1)
		6.48	$7/2^-,1/2$	d	6.74	$7/2^-,1/2$	(3/2/1)
		12.47	$1/2^-,3/2$	0	12.94	$1/2^-,3/2$	(0/0/0)

[a] $E_p^{\rightarrow}$ is the beam energy in MeV lab.

[b] J^π,T assignments and excitation energies are from Ref. 19 except for the ^{14}O 9.72 MeV state from Ref. 6 and the T = 3/2 analog states in mass-11 from Ref. 20.

(continued)

Table II (continued)

[c]Two-nucleon cfp's were not available for these negative parity states in Ref. 16.

Shell model configurations were based on Ref. 17 as follows:

$$|^{14}O^*(5.17),\ 1^-> = |[p_{1/2}\ s_{1/2}]_{1^-}>$$

$$|^{14}O^*(6.29),\ 3^-> = |[p_{1/2}\ d_{5/2}]_{3^-}>$$

$$|^{14}N^*(5.11),\ 2^-> = |[p_{1/2}\ d_{5/2}]_{2^-}>$$

[d]This transition is L-forbidden. See text.

FIGURE CAPTIONS

Fig. 1. Analyzing powers of the four pairs of analog transitions observed in this work. Each pair is identified by the target and the final state J^{π},T.

Fig. 2. Energy spectra for the $^{16}O(\vec{p},t)^{14}O$ and $^{16}O(\vec{p},^{3}He)^{14}N$ reactions.

Fig. 3. Differential cross sections (left) and analyzing powers for transitions observed in the $^{16}O(\vec{p},t)^{14}O$ reaction. The curves are DWBA calculations described in the text, and are separately and arbitrarily normalized to the data for $\frac{d\sigma}{d\Omega}$ only.

Fig. 4. Differential cross sections (left) and analyzing powers for observed $^{16}O(\vec{p},^{3}He)^{14}N$ transitions. The curves are obtained from DWBA calculations described in the text, and are separately and arbitrarily normalized to the data for $\frac{d\sigma}{d\Omega}$ only.

Fig. 5. Energy spectra for the $^{15}N(\vec{p},t)^{13}N$ and $^{15}N(\vec{p},^{3}He)$ reactions.

Fig. 6. Differential cross sections (left) and analyzing powers for $^{15}N(\vec{p},t)^{13}N$ transitions observed. DWBA calculations discussed in the text are shown by the curves, and are separately and arbitrarily normalized to the $\frac{d\sigma}{d\Omega}$ data only.

Fig. 7. Differential cross sections (left) and analyzing powers for $^{15}N(\vec{p},^{3}He)$ transitions to states in ^{13}C. The curves show DWBA calculations described in the text, which are separately and arbitrarily normalized to the $\frac{d\sigma}{d\Omega}$ data only.

Fig. 8. Energy spectra for the $^{13}C(\vec{p},t)^{11}C$ and $^{13}C(\vec{p},^{3}He)^{11}B$ reactions.

Fig. 9. Differential cross sections (left) and analyzing powers for the $^{13}C(\vec{p},t)^{11}C$ transitions to several final states. The curves are DWBA calculations described in the text, and are separately and arbitrarily normalized to the $\frac{d\sigma}{d\Omega}$ data only.

Fig. 10. Differential cross sections (left) and analyzing powers for transitions observed in $^{13}C(\vec{p},{}^{3}He)$ to final states in ^{11}B. The curves show DWBA calculations discussed in the text, and are separately and arbitrarily normalized to the data for $\frac{d\sigma}{d\Omega}$ only.

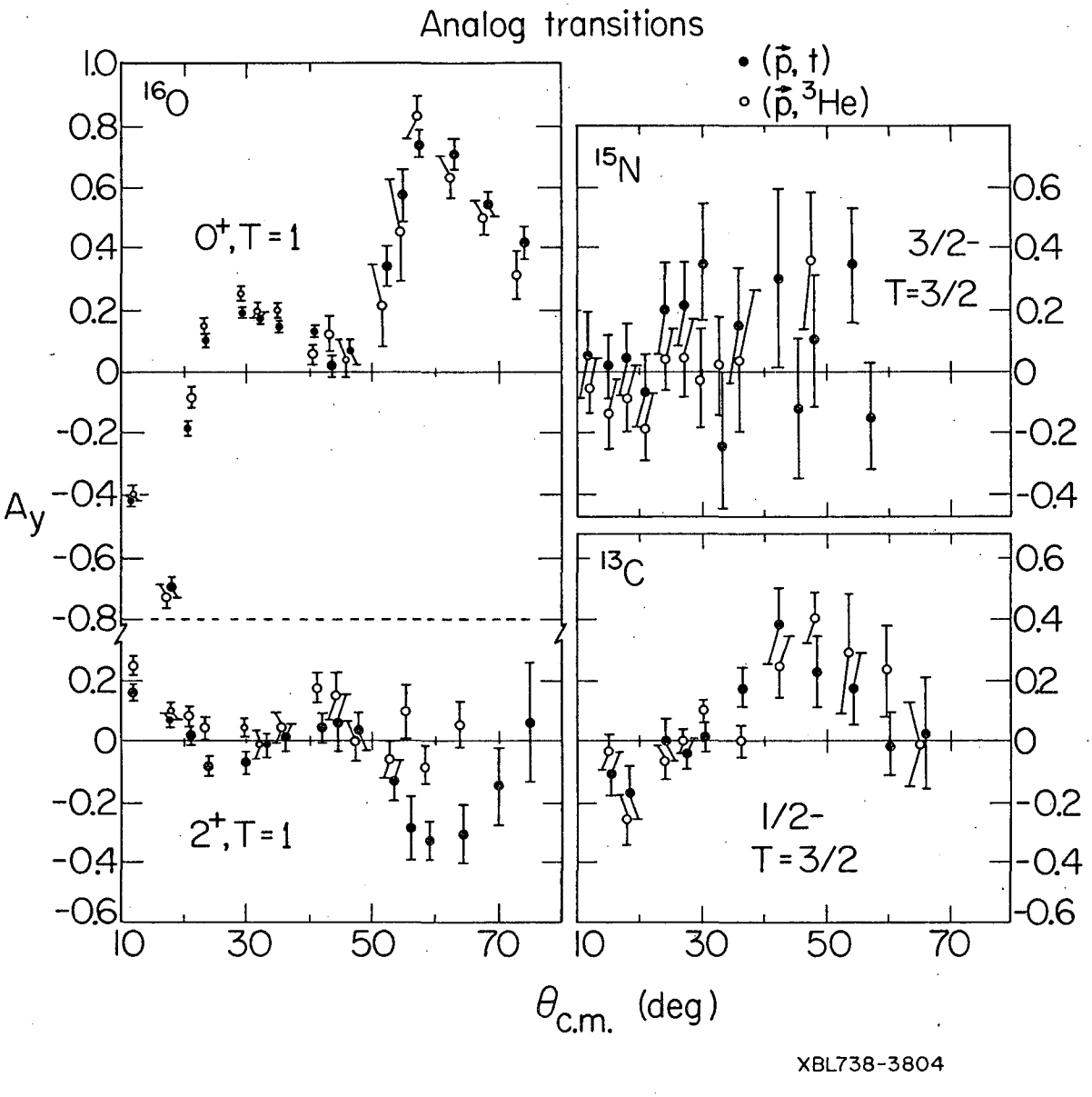
Analog transitions
• (p⃗, t)
∘ (p⃗, ³He)
¹⁶O
0⁺, T = 1
2⁺, T = 1
¹⁵N
3/2⁻
T=3/2
¹³C
1/2⁻
T = 3/2
Ay
θc.m. (deg)
XBL738-3804

Fig. 1

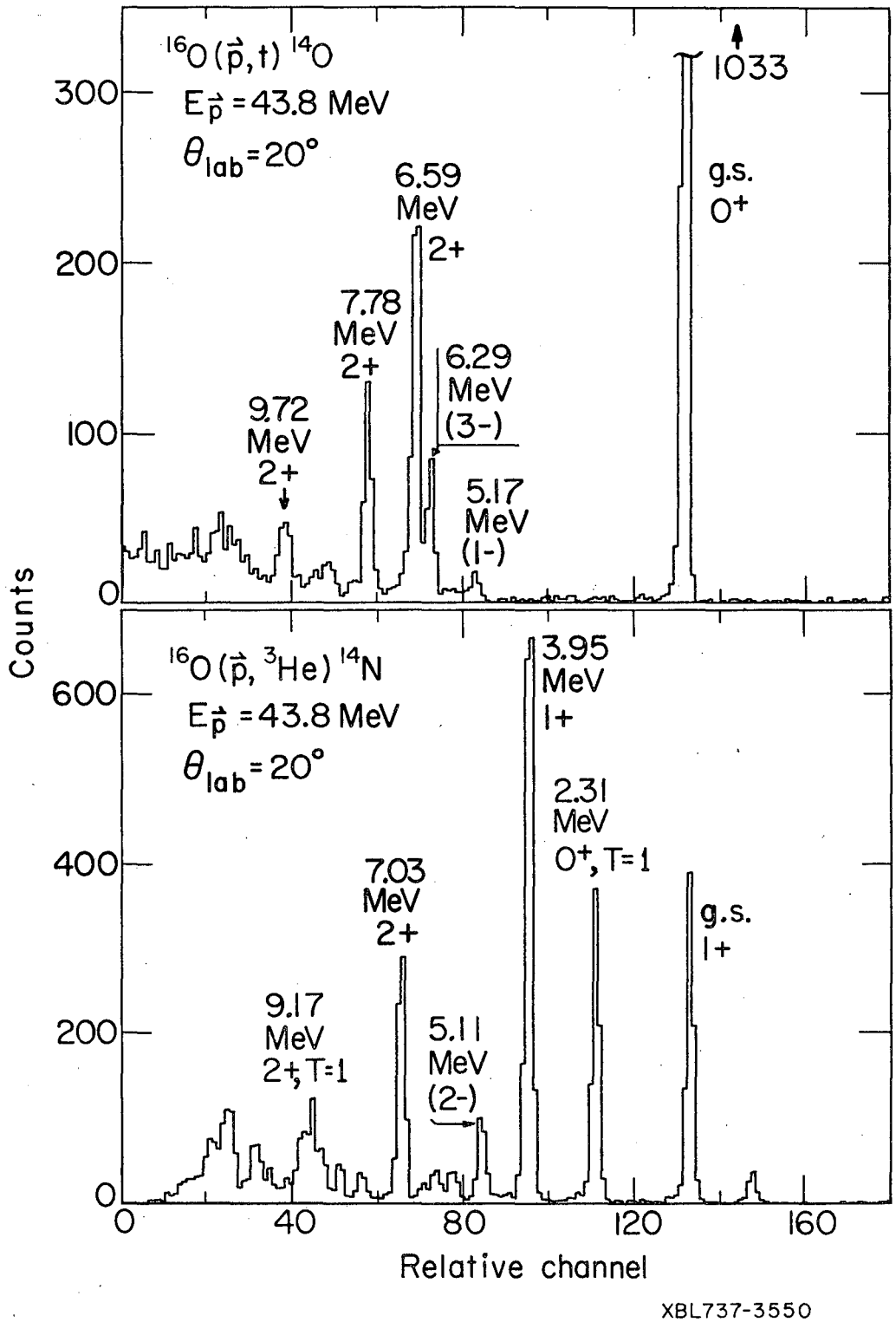
$^{16}O(\vec{p},t)\,^{14}O$
$E_{\vec{p}}$ = 43.8 MeV
θ_{lab} = 20°
1033
g.s.
0+
6.59
MeV
2+
7.78
MeV
2+
6.29
MeV
(3-)
9.72
MeV
2+
5.17
MeV
(1-)
300
200
100
0
$^{16}O(\vec{p},{}^{3}He)\,^{14}N$
$E_{\vec{p}}$ = 43.8 MeV
θ_{lab} = 20°
3.95
MeV
1+
2.31
MeV
0+, T=1
7.03
MeV
2+
g.s.
1+
9.17
MeV
2+, T=1
5.11
MeV
(2-)
600
400
200
0
Counts
0
40
80
120
160
Relative channel
XBL737-3550

Fig. 2

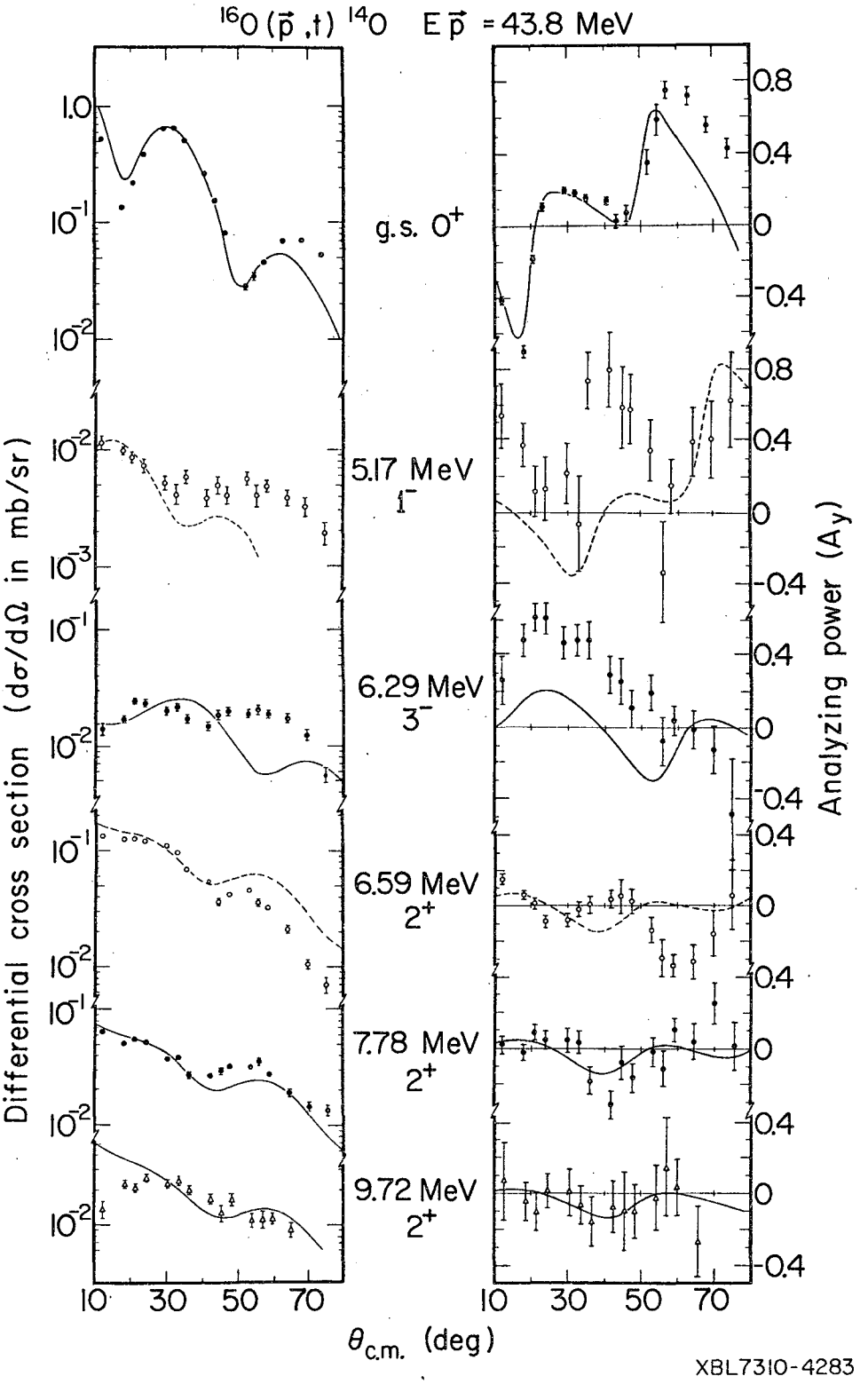
$^{16}O(\vec{p},t)^{14}O$ $E\vec{p}$ = 43.8 MeV
g.s. 0^+
5.17 MeV
1^-
6.29 MeV
3^-
6.59 MeV
2^+
7.78 MeV
2^+
9.72 MeV
2^+
Differential cross section ($d\sigma/d\Omega$ in mb/sr)
Analyzing power (A_y)
$\theta_{c.m.}$ (deg)
XBL7310-4283

Fig. 3

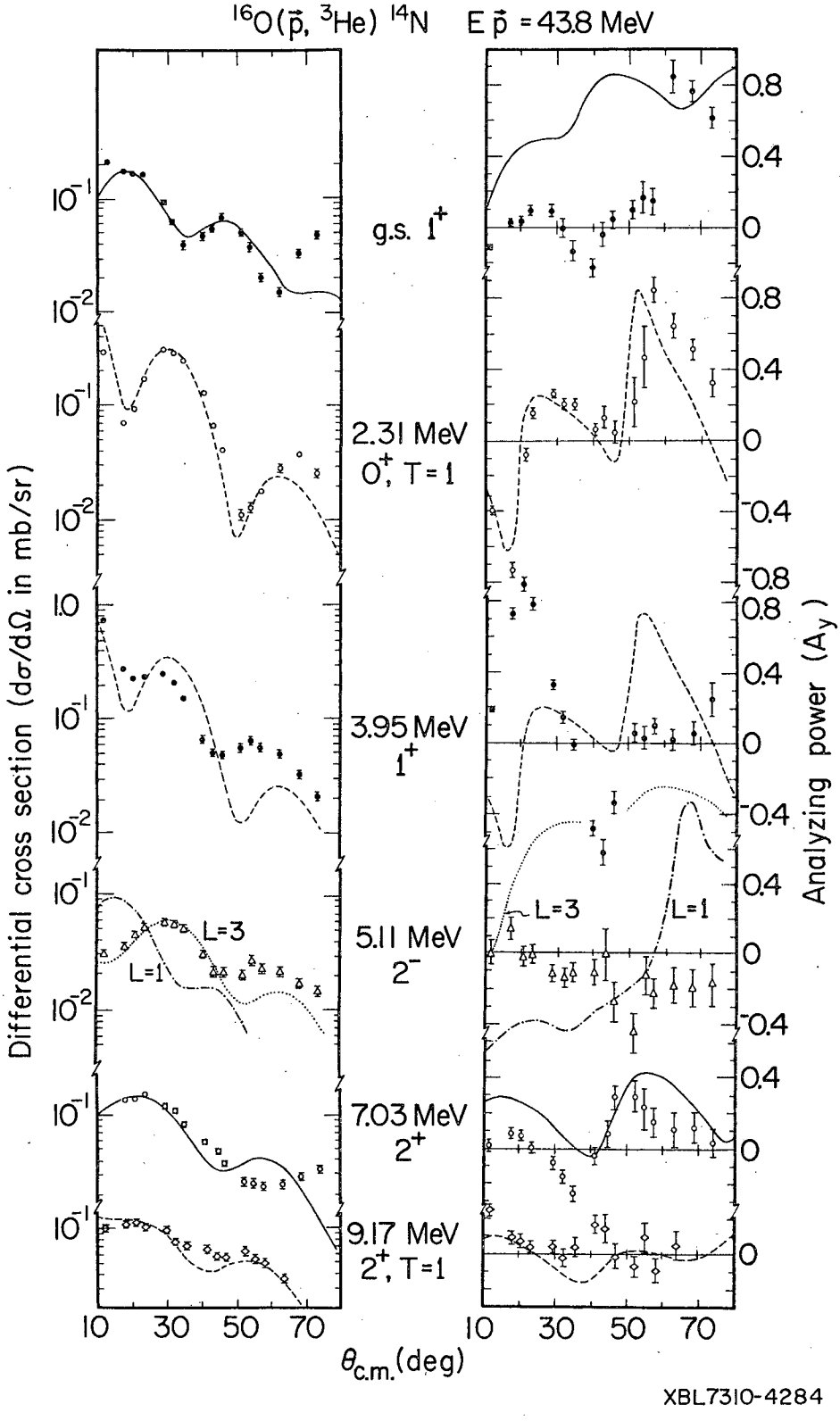
$^{16}O(\vec{p}, {}^{3}He)\ ^{14}N$ $E\vec{p}$ = 43.8 MeV
g.s. 1^+
2.31 MeV
0^+, T=1
3.95 MeV
1^+
5.11 MeV
2^-
7.03 MeV
2^+
9.17 MeV
2^+, T=1
L=3
L=1
Differential cross section ($d\sigma/d\Omega$ in mb/sr)
Analyzing power (A_y)
$\theta_{c.m.}$(deg)
XBL7310-4284

Fig. 4

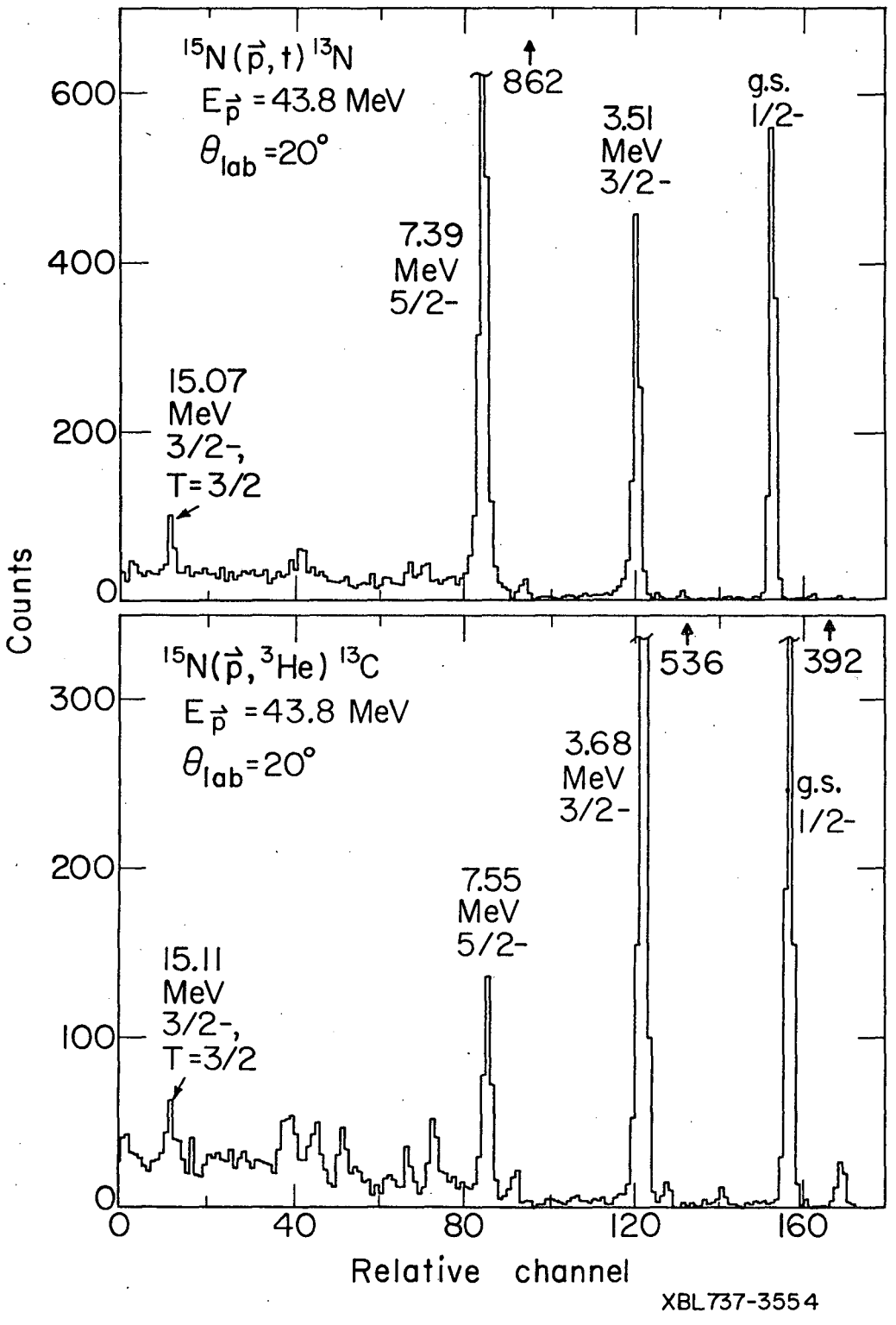
$^{15}N(\vec{p},t)^{13}N$
$E_{\vec{p}}$ = 43.8 MeV
θ_{lab} = 20°
862
g.s.
1/2-
3.51
MeV
3/2-
7.39
MeV
5/2-
15.07
MeV
3/2-,
T=3/2
$^{15}N(\vec{p},{}^3He)^{13}C$
$E_{\vec{p}}$ = 43.8 MeV
θ_{lab} = 20°
536
392
3.68
MeV
3/2-
g.s.
1/2-
7.55
MeV
5/2-
15.11
MeV
3/2-,
T=3/2
Counts
0
100
200
300
400
600
0
40
80
120
160
Relative channel
XBL737-3554

Fig. 5

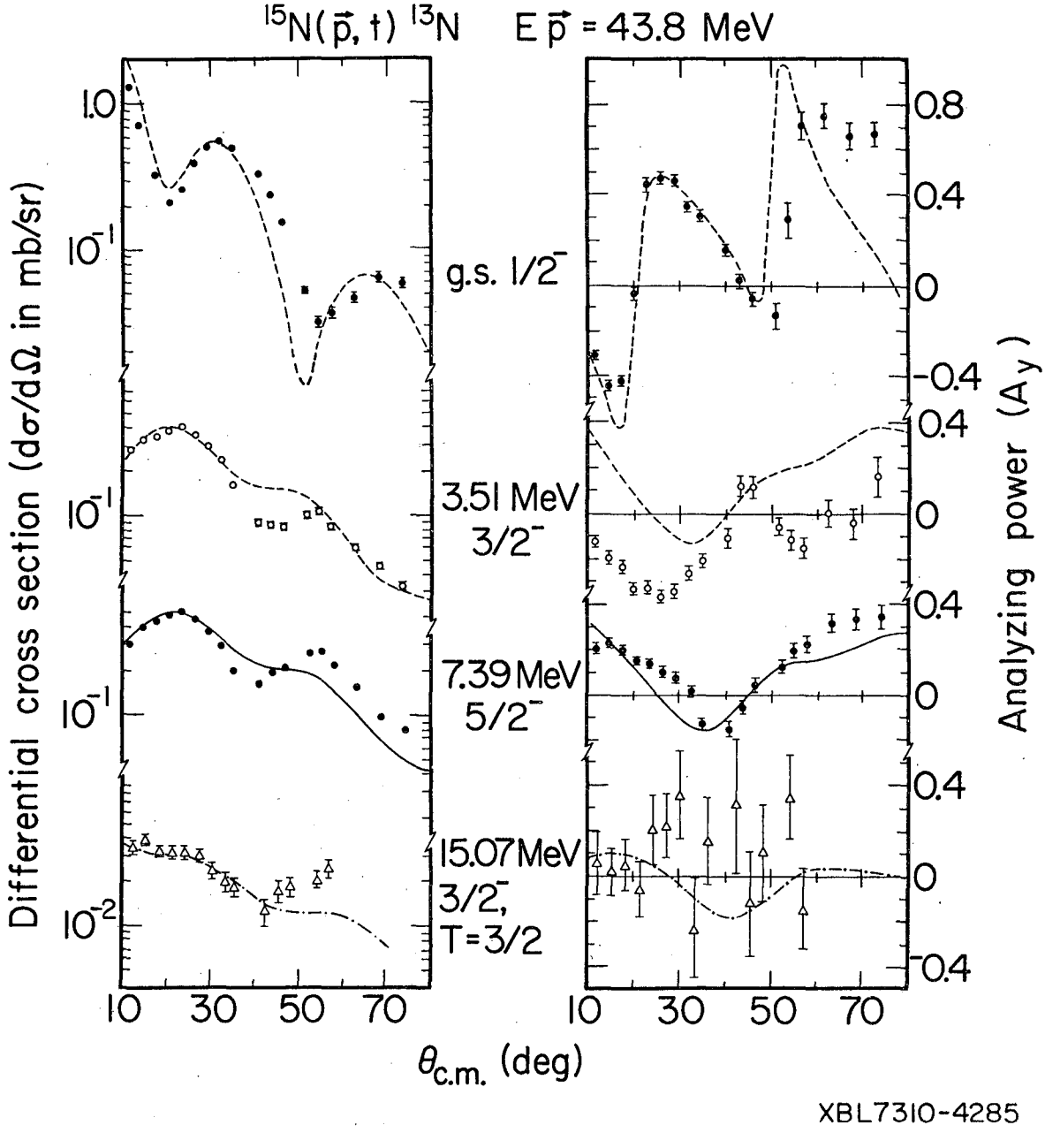
$^{15}N(\vec{p}, t)\ ^{13}N$ $E\vec{p}$ = 43.8 MeV
Differential cross section (dσ/dΩ in mb/sr)
Analyzing power (A_y)
g.s. 1/2⁻
3.51 MeV 3/2⁻
7.39 MeV 5/2⁻
15.07 MeV 3/2⁻, T=3/2
$\theta_{c.m.}$ (deg)
XBL7310-4285

Fig. 6

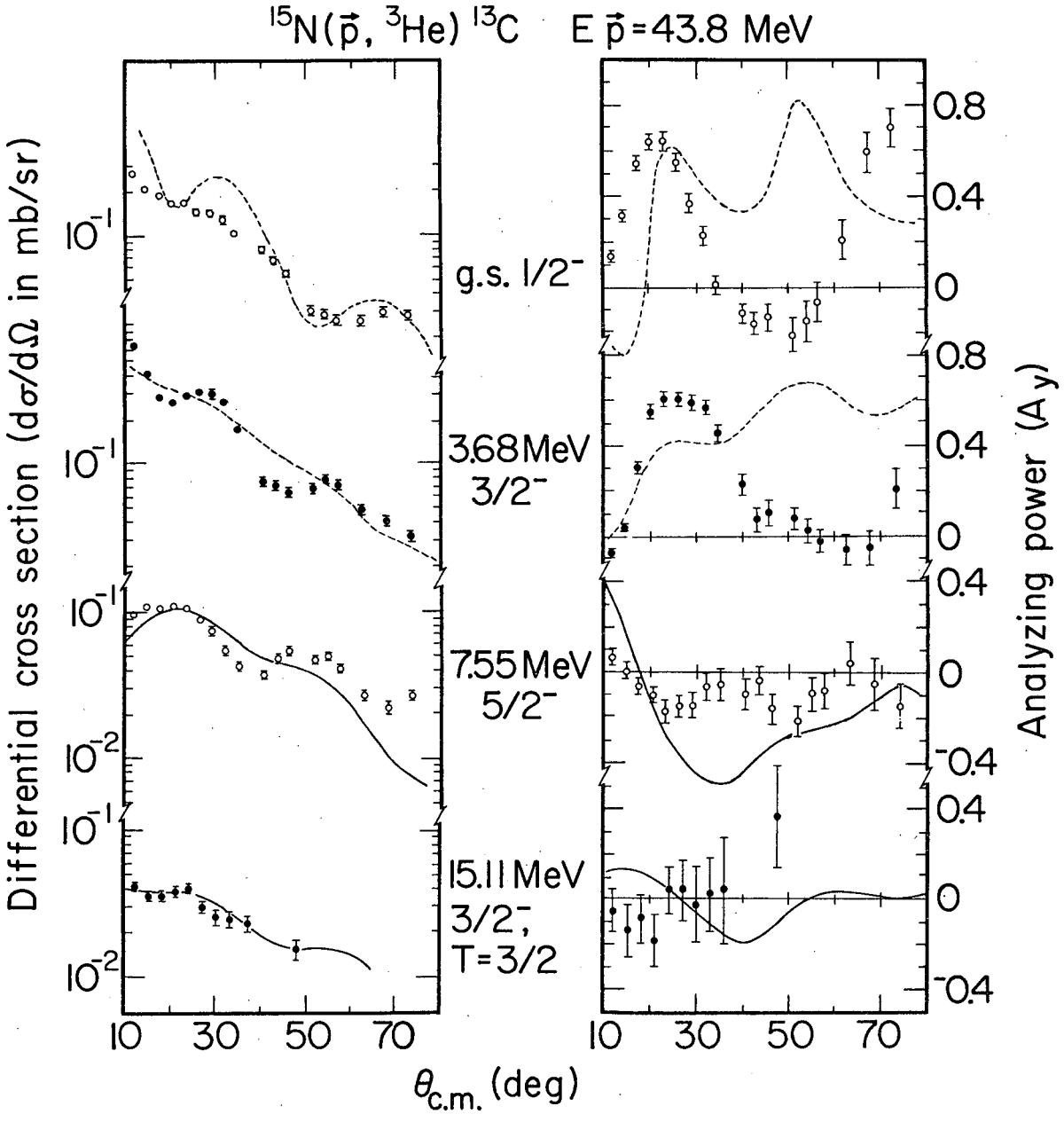
$^{15}N(\vec{p}, {}^{3}He)\,{}^{13}C$ E $\vec{p}$=43.8 MeV
Differential cross section (dσ/dΩ in mb/sr)
Analyzing power (A_y)
g.s. 1/2⁻
3.68 MeV 3/2⁻
7.55 MeV 5/2⁻
15.11 MeV 3/2⁻; T=3/2
$\theta_{c.m.}$ (deg)
10 30 50 70
0.8 0.4 0 -0.4
XBL7310-4286

Fig. 7

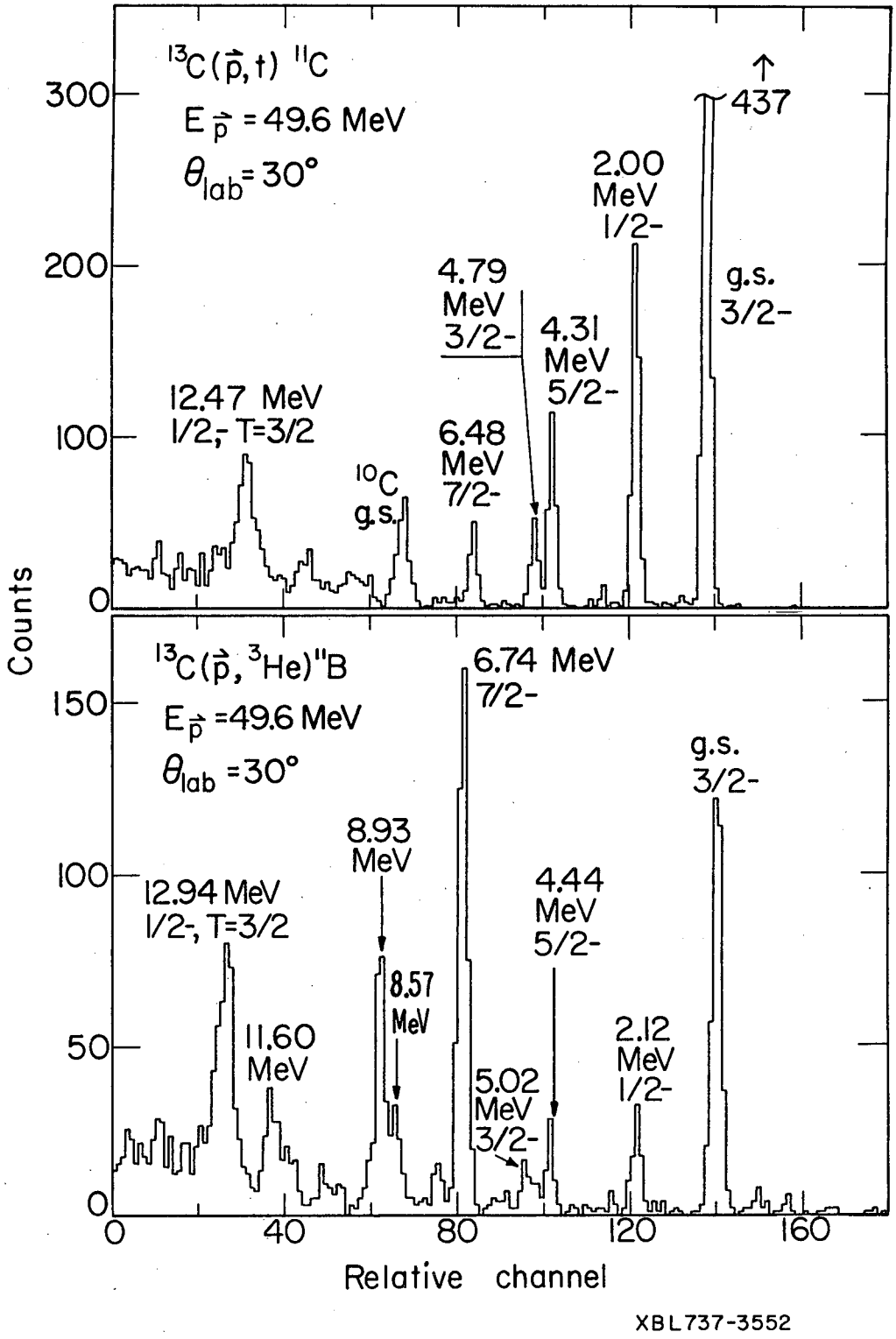
$^{13}C(\vec{p},t)\ ^{11}C$
$E_{\vec{p}}$ = 49.6 MeV
θ_{lab} = 30°
437
2.00 MeV 1/2-
g.s. 3/2-
4.79 MeV 3/2-
4.31 MeV 5/2-
12.47 MeV 1/2-; T=3/2
^{10}C g.s.
6.48 MeV 7/2-
$^{13}C(\vec{p},{}^3He)^{11}B$
$E_{\vec{p}}$ = 49.6 MeV
θ_{lab} = 30°
6.74 MeV 7/2-
g.s. 3/2-
8.93 MeV
12.94 MeV 1/2-, T=3/2
4.44 MeV 5/2-
8.57 MeV
11.60 MeV
2.12 MeV 1/2-
5.02 MeV 3/2-
Counts
Relative channel
0
40
80
120
160
XBL737-3552

Fig. 8

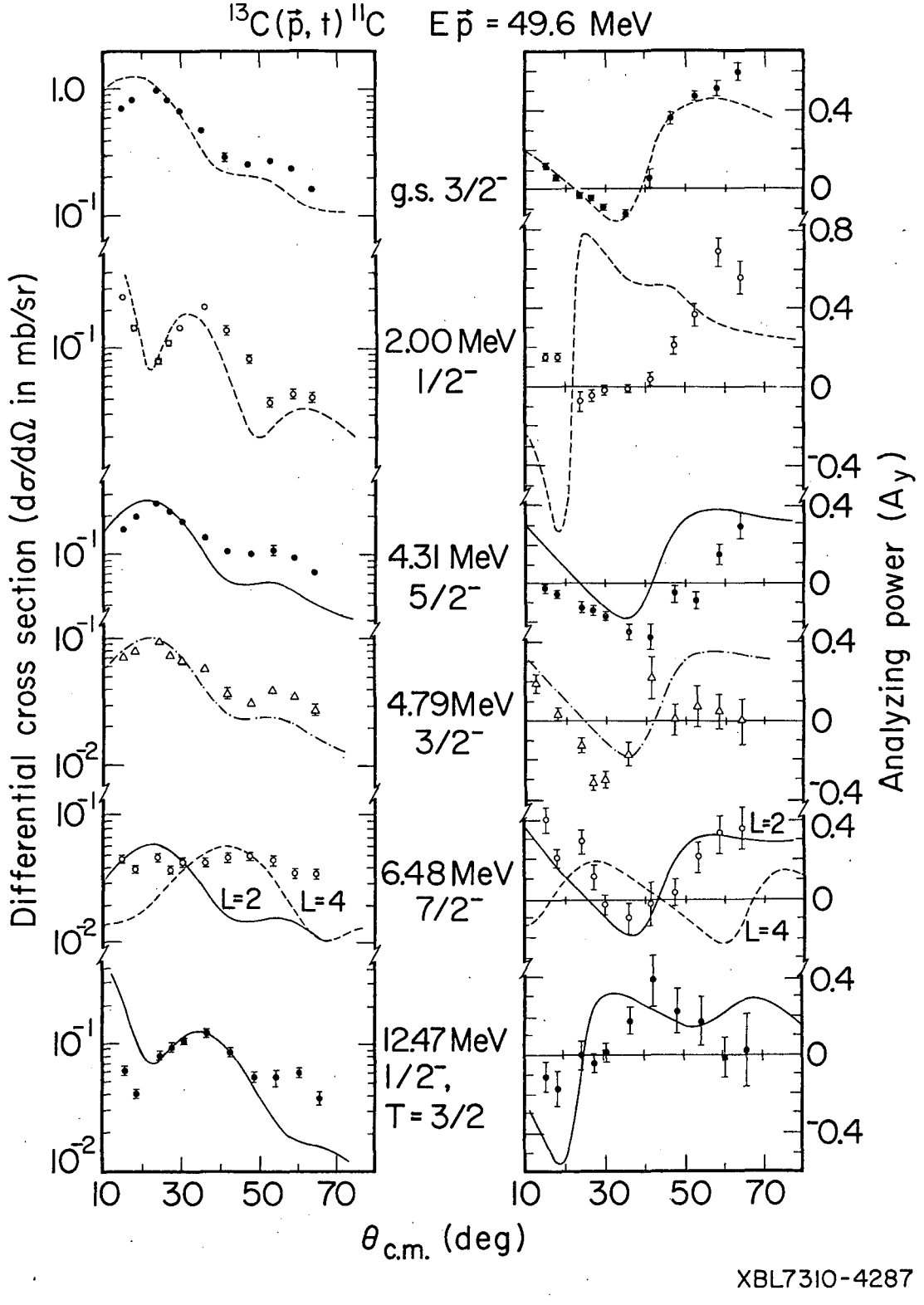
$^{13}C(\vec{p}, t)\,^{11}C$ $E\vec{p}$ = 49.6 MeV
Differential cross section ($d\sigma/d\Omega$ in mb/sr)
Analyzing power (A_y)
$\theta_{c.m.}$ (deg)
g.s. 3/2⁻
2.00 MeV 1/2⁻
4.31 MeV 5/2⁻
4.79MeV 3/2⁻
6.48 MeV 7/2⁻
12.47 MeV 1/2⁻, T = 3/2
L=2
L=4
XBL7310-4287

Fig. 9

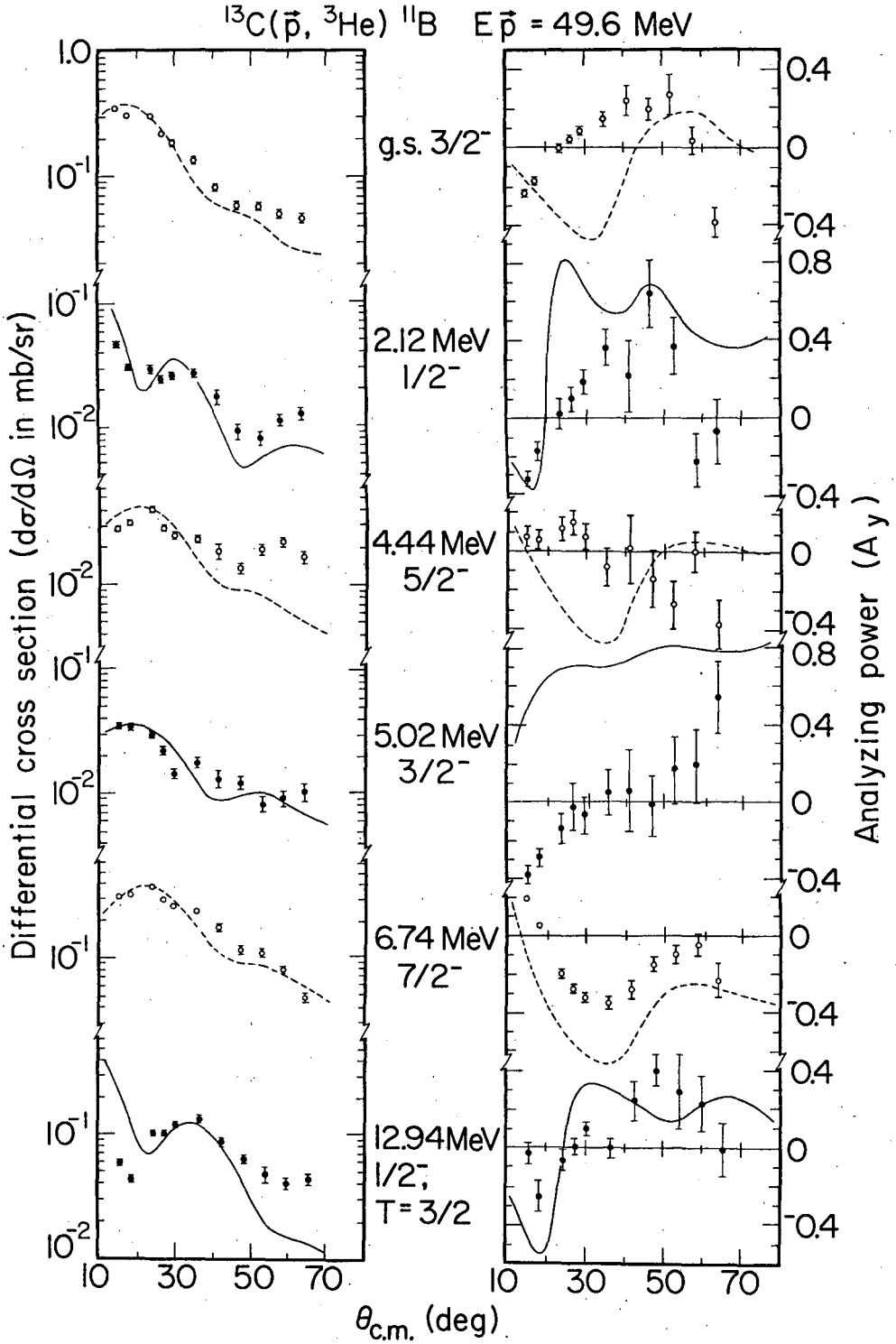
$^{13}C(\vec{p}, {}^3He)\ ^{11}B$ $E\vec{p}$ = 49.6 MeV
g.s. 3/2⁻
2.12 MeV 1/2⁻
4.44 MeV 5/2⁻
5.02 MeV 3/2⁻
6.74 MeV 7/2⁻
12.94MeV 1/2⁻; T= 3/2
Differential cross section (dσ/dΩ in mb/sr)
Analyzing power (A_y)
θc.m. (deg)
XBL7310-4288

Fig. 10

TECHNICAL INFORMATION DIVISION
LAWRENCE BERKELEY LABORATORY
UNIVERSITY OF CALIFORNIA
BERKELEY, CALIFORNIA 94720